Langmuir

Article

pubs.acs.org/Langmuir

Control of Ordering and Structure in Soft Templated Mesoporous Carbon Films by Use of Selective Solvent Additives

Zhe Qiang,[†] Jiachen Xue,[†] Gila E. Stein,[‡] Kevin A. Cavicchi,[†] and Bryan D. Vogt*[,†]

[†]Department of Polymer Engineering, University of Akron, Akron, Ohio 44325, United States

[‡]Department of Chemical and Biomolecular Engineering, University of Houston, Houston, Texas 77204, United States

Supporting Information

ABSTRACT: The structure of ordered mesoporous carbons fabricated using poly(styrene-block-*N*,*N*,-dimethyl-*n*-octadecylamine *p*-styrenesulfonate) (PS-*b*-PSS-DMODA) as the template and phenolic resin (resol) as the carbon source can be easily manipulated by inclusion of low concentrations of low volatility selective solvents in the casting solution. Casting from neat methyl ethyl ketone yields a disordered structure even upon thermal annealing. However, addition of both dioctyl phthalate (DOP, PS selective) and dimethyl sulfoxide (DMSO, resol and PSS-DMODA selective) at modest concentrations to this casting solution provides sufficient mobility to produce highly ordered films with cylindrical mesopores. The DOP acts to swell the hydrophobic domain and can more than double the mesopore size, while the DMSO acts to swell the resol phase. Moreover, the surface area of the mesoporous carbons increases significantly as the meosopore size increases. This is a result of the decrease in wall thickness, which can be ascertained by the constant *d*-spacing of the mesostructure as the pore size increases. This behavior is counter to the typical effect of pore swelling agents that increase the pore size and decrease the surface area. Moreover, with only 4 wt % DOP/DMSO in the solution (20 wt % relative to solids), the scattering profiles exhibit many orders of diffraction, even upon carbonization, which is not typically observed for soft templated films. Variation in the concentration of DOP and DMSO during casting enables facile tuning of the structure of mesoporous carbon films.

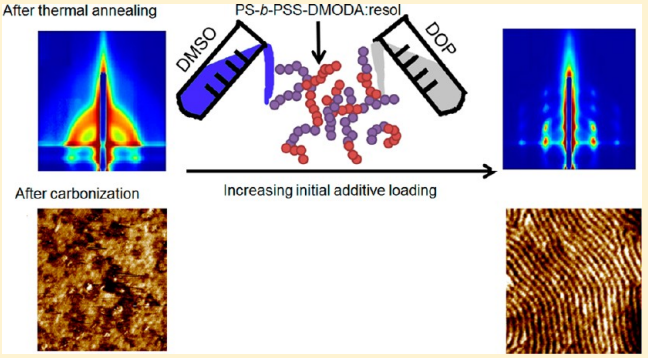

INTRODUCTION

Well-defined mesoporous carbon materials have received increasing interest due to their broad potential in applications such as gas separation,[1,2] water purification,[3] catalysis,[4,5] controlled drug delivery,[6,7] energy storage,[8] and electrodes for batteries.[9,10] Two general routes for the synthesis of ordered mesoporous carbon materials exist. Hard-templating[11] requires multiple steps to fabricate the mesoporous carbon with synthesis of an inorganic (silica) master, infiltration of precursor, carbonization, and finally template removal.[12,13] Alternatively, soft-templating involves the coassembly of carbonizable precursors with an amphiphilic surfactant or block copolymer to yield an ordered and uniform mesostructure.[14,15] Zhao and co-workers have demonstrated this method using commercially available Pluronic block copolymer (e.g., F127 and P123)[16] or amphiphilic diblock copolymers[17−19] as templates and phenolic resin oligomer (resol) as the carbon source. In most cases, these ordered porous carbons are produced as powders,[13,20] but there are a number of applications where thin film coatings[21] or free-standing membranes[22,23] would be preferred.

In thin films, the soft-templating approach can be readily applied to synthesize highly ordered mesoporous carbon thin films,[24,25] but the mechanism for mesostructure formation using resol as the carbon precursor is thermally induced self-assembly (TISA)[26] instead of the typical evaporation induced self-assembly (EISA), which is common for sol−gel based mesoporous films.[27,28] TISA is a common ordering process for neat block copolymer systems,[29] which opens the potential for using block copolymer process routes to modify or modulate the structure of mesoporous carbons.

In TISA, the thermal energy that leads to ordering the mesostructure also drives cross-linking of the resol. The competition between ordering kinetics and cross-linking can lead to a poorly ordered structure in films in some cases.[30] For example, poly(styrene-*block*-ethylene oxide) (PS-*b*-PEO)/resol yields well-ordered mesosturctures for powders,[31] while poorly ordered structures are obtained in analogous thin films.[32] An extreme example is using ionic templates where the strong interaction between resol and the template leads to limited ordering ability for the system. An alternative for ordering is solvent vapor annealing. Dai and co-workers previously used saturated solvent swelling and subsequent slow evaporation (24 h) to obtain vertically oriented cylindrical mesoporous carbon

Received: April 20, 2013
Revised: June 4, 2013
Published: June 5, 2013

   dx.doi.org/10.1021/la401505h | *Langmuir* 2013, 29, 8703−8712

through a block copolymer templating approach.[14] We have recently demonstrated that controlled solvent vapor annealing (SVA) using mass flow controllers to tune the solvent swelling is a facile route to overcome the limitations of TISA and achieve longer range order and narrower pore size distributions with shorter annealing times (2 h).[33] The samples order by swelling polymer chains with solvent and subsequently the mesostructure is fixed by cross-linking the resol. However, the ordering of the films during cross-linking decreases markedly, which is similar to the block copolymer systems that cross-link.[34] A major challenge is that SVA is difficult to scale to commercial settings due to the large concentration of organic vapor required that provide substantial safety and health risks.

One intriguing observation from this solvent vapor annealing work is that residual neutral good solvent in the film after SVA enables significant reordering of the template during thermal cross-linking.[33] Low volatility solvent additives have been utilized in the synthesis of mesoporous materials previously,[35,36] but these additives have generally been hydrophobic to swell the micelles and increase the pore size. Wickramaratne and Jaroniec have recently demonstrated that this approach also applies to soft templated carbons.[37] However, this solvent additive approach for the synthesis of mesoporous materials only modulated the size of the mesopores without significantly impacting the ordering of these materials. Alternatively, the mesopores size for carbon powders can be increased by addition of an appropriate hydrophobic polymer,[38] but extension to thin films is ineffective due to surface segregation (wetting) of the polymer.[32]

Here, we propose a novel, industrially relevant approach to improve the ordering and modulate the structure of mesoporous carbon films through the use of mixed solvent additives (high boiling point solvents) in the solution prior to film casting. Specifically, an ionic block copolymer template, poly(styrene-*block*-*N*,*N*-dimethyl-*n*-octadecylamine *p*-styrenesulfonate) (PS-*b*-PSS-DMODA), is used for fabricating mesoporous carbon thin films due to prior success with SVA[33] in obtaining a highly ordered mesostructure. In this case, the mixed additives, dioctyl phthalate (DOP) and dimethyl sulfoxide (DMSO), provide sufficient mobility to enhance the long-rang ordering during thermal annealing while cross-linking the resol. The residual solvent in films after thermal annealing can be totally removed during calcination or carbonization. The use of two highly selective solvents prevents significant compatibilization of the block copolymer that can occur with a single neutral solvent.[39] The results demonstrate that this facile approach enables highly ordered mesoporous films with near invariance of the *d*-spacing. Despite no change in *d*-spacing, these cosolvents can effectively tune the pore size and surface area with both increasing with solvent concentration. This mixed solvent approach for fabrication of mesoporous carbon films provides a facile, scalable solution to enabling highly ordered films with tunable control of physical properties, in particular for the synthesis of thin films with large ordered mesopores.

EXPERIMENTAL SECTION

Materials. Sodium *p*-styrenesulfonate (NaSS), chlorobenzene (>99.8%), dimethyl sulfoxide (DMSO) (>99.8% HPLC grade), bis(2-ethylhexyl) phthalate (DOP) (>98%) and styrene (>99% stab. with 10−15 ppm 4-tert-butylcatechol) were purchased from Alfa Aesar company. *N*,*N*-Dimethyl-*n*-octadecylamine (DMODA) was purchased from Tokyo Chemical Industry Co. Ltd (>85%). Tetrahydrofuran (THF) (>99%), phenol (>99%), and formaldehyde (ACS reagent, 37 wt % in H_2O, contains 10−15% methanol as stabilizer) were purchased from Sigma-Aldrich. Methyl-ethyl-ketone (MEK) (>99%) and hexane (>99%) were purchased from Fisher Scientific. Sodium hydroxide (>99%) was purchased from EMD Chemicals Inc. Nitrogen gas (>99%) was purchased from Praxair and used in both the polymer synthesis and carbonization. Styrene was purified by filtering through a basic Al_2O_3 column to remove the polymerization inhibitor. All other reagents were used as-received.

A cross-linkable, low-molecular weight phenolic resin (resol) was synthesized using phenol and formaldehyde (37 wt % in H_2O) in the presence of a base catalyst as described previously.[16] After condensation for 1 h at 73 °C, dilute HCl (1 M) was used to neutralize the solution at room temperature (pH ∼7). The water was removed by rotatory evaporation at low temperatures (<49 °C) to prevent cross-linking of the resol. Then dry resol was dissolved in methyl ethyl ketone (MEK) and NaCl salt precipitants were filtered out.

Synthesis of PS-*b*-PSS-DMODA. Poly(styrene)-*block*-poly(*N*,*N*-dimethyl-*n*-octadecylamine *p*-styrenesulfonate) (PS-*b*-PSS-DMODA) (65 mol % PS (^{1}H NMR), M_n = 10.2 kDa and Đ = 1.26 (size exclusion chromatography calibrated by PS standards), $T_d \approx 300$ °C (TGA)) served as the block copolymer template and its preparation by reversible addition−fragmentation chain transfer (RAFT) polymerization was previously reported.[33]

Film Preparation and Processing. PS-*b*-PSS-DMODA (template) and resol (precursor) were mixed at a mass ratio of 1:3 (selected to mimic ∼80% hydrophilic fraction and dissolved in methyl ethyl ketone (MEK) at 20 wt % solid). For the mixed solvent processing, DMSO and DOP were first mixed at a mass ratio of 4:1 and added into the PS-*b*-PSS-DMODA:resol solution in MEK at 5, 10, 15, or 20 wt % relative to PS-*b*-PSS-DMODA:resol content. This specific ratio of DMSO and DOP of 4:1 was selected to maintain a constant hydrophilic−hydrophobic ratio of the PS-*b*-PSS-DMODA:resol films. The nomenclature of these films is PR-*x*, where *x* is the mass fraction of mixed solvents relative to solids content. Control experiments involving no solvent additive and only DOP or DMSO as the additive to the solution were also performed.

Silicon wafers with a 300 nm thermal oxide layer (University Wafer) were used as substrates and were cleaned with UV ozone (Jelight Company Inc., model no. 42) for 1 h prior to use. Films of PS-*b*-PSS-DMODA:resol were spin coated from solution onto silicon wafers at 3500 rpm for 1 min. Then, the films were heated at 160 °C for 24 h to cross-link the phenolic resin and induce ordering of the mesostructures. After cross-linking the resol, mesoporous polymer thin films were obtained by removing the template at 400 °C for 3 h in N_2 atmosphere using a heating rate of 1.5 °C/min. To fabricate mesoporous carbon films, a ramp rate of 1.5 °C/min below 400 and 4 °C/min above 400 °C was utilized with an ultimate hold temperature of 800 °C for 3 h.

Characterization of Thin Films. A variable angle spectroscopic ellipsometer (VASE, J.A. Woollam Co., M-2000) was used to obtain the optical constants (*n*, *k*) and thickness of the films. General scans were performed at multiple incident angles (65°, 70°, and 75°) over the wavelength range from 246 to 1689 nm. The data were fit using a model consisting of the silicon substrate (containing an interface layer and SiO_2 layer for the oxide) and a Cauchy layer to describe the polymeric films. For carbonized films, the large absorption in the visible regime was fit with a general oscillator model consisting of Gaussian and Lorenzian functions. Ellipsometric porosimetry (EP)[40] was utilized to determine the pore size distribution (PSD) with toluene used as the probe solvent for condensation in the pores of the film. The associated changes in refractive index from capillary condensation were investigated by in situ ellipsometry using a cell with fixed 70° quartz windows while measuring both absorption and desorption isotherms.[41,42] The surface morphology of the films after templates removal and carbonization was investigated by atomic force microscopy (AFM, Dimension ICON, Veeco). Phase images (2 μm × 2 μm) were obtained using tapping mode at 0.5 Hz with PPP-NCC-50 tips (Nanosensors). Grazing incidence small-angle X-ray scattering

dx.doi.org/10.1021/la401505h | *Langmuir* 2013, 29, 8703−8712

(GISAXS) measurements were performed at the X9 beamline of the National Synchrotron Light Source (NSLS) at Brookhaven National Laboratory (BNL) and beamline 8-ID-E at the Advanced Photon Source (APS) of Argonne National Laboratory. At NSLS, an incident X-ray beam of energy 13.5 keV (wavelength (λ) = 0.0918 nm) was used at a sample-to-detector distance of 4.73 m. All of the films were measured below and above critical angle under vacuum. At APS, samples under vacuum were illuminated with 7.35 keV radiation at incident angles (α_i) in the range of 0.1°−0.24°; the off-specular scattering was recorded with a Pilatus 1MF pixel array detector (pixel size = 172 μm) positioned 2175 mm from the sample. Acquisition times were approximately 10 s per frame. Each data set was stored as a 981 × 1043 32-bit tiff image (20 bit dynamic range). The GISAXS data in both cases are presented as a function of the two representative momentum transfer vectors, q_z and q_x:

$$q_z = k_0(\sin \alpha_i + \sin \alpha_f)$$

$$q_x = k_0 \sin(2\theta)$$

$$k_0 = \frac{2\pi}{\lambda}$$

where α_f and 2θ are the scattering angles with respect to the out-of-plane (z) and in-plane (x) directions (see the Supporting Information for more details).

RESULTS AND DISCUSSION

For fabricating optically smooth and uniform films, methyl ethyl ketone (MEK) is selected as the primary solvent as it is a good solvent for all the components (PS block, PSS-DMODA block and resol). The selected additives, DMSO and DOP, are low-volatility solvents, which are difficult to remove from the polymer films at room temperature. Thus after spin-coating, significant residual solvent remains in the films to enhance the chain mobility during thermal annealing and cross-linking at 160 °C. To illustrate that these low volatility solvents impact film formation, Figure 1 shows the thicknesses of the films after different stages in processing from spin coating to carbonization.

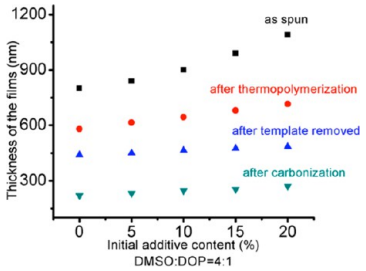

Figure 1. Thickness of films for (black square) as-spun; (red circle) after thermopolymerization, (blue triangle) after template removal, and (green triangle) after carbonization as a function of solvent additive content.

For the spun-cast films, there is an increase in thickness with increasing mass fraction of the solvent additives. The thickness of the as-spun PR-0 film is 800 nm and increases to 1090 nm for PR-20; this is a 38% increase in thickness, which is more than the solvent content in the solution. This difference can be attributed to the differences in the rheological properties from the solvent changes that may promote ordering as the MEK evaporates during spin coating due to the high selectivity of these solvent additives.[43] As the equilibrium concentration of solvents in block copolymers can be different between the ordered and disordered states,[44] the concentrations of DOP and DMSO in the films may be altered from the initial solution. These hypotheses are supported by the concentration dependent change in thickness that deviates from a simple 1:1 correlation as the concentration of solvent additives (DMSO and DOP) increases. However when the solvent additives are present at greater than 25 wt % relative to solids, the film dewets rapidly after spin-coating (see Figure S1 in the Supporting Information). We have previously demonstrated that PS-*b*-PSS-DMODA:resol films dewet at high solvent concentrations when using solvent vapor annealing with MEK with an upper swelling limit of 36%,[33] which is very similar to the 38% increase in thickness illustrated in Figure 1 with the addition of DMSO and DOP. Thus, for fabricating well-ordered mesoporous films, the content of the solvent additives need to be selected in order to maintain a stable film. After thermal annealing at 160 °C for 24 h, the film thickness appears to be linearly related to the initial fraction of DMSO and DOP in the casting soluion. For example, the PR-20 film is approximately 23% thicker than PR-0. For carbonizaion, the contraction from mesoporous polymer to carbon (45%) is independent of the initial casting solution composition as all the residual solvent is removed prior to the carbonization step.

To examine how these solvent additives impact the mesostructure, GISAXS profiles are obtained as a function of the processing conditions. First, Figure 2 illustrates the GISAXS patterns for thermally annealed films, which show obvious differences in the structure for different solvent additive loadings. As shown in Figure 2A without any low volatility solvent, the scattering pattern shows weak peaks in q_x with the primary peak at $q_x \approx 0.27$ nm^{-1} with a very weak second order reflection; this scattering is consistent with hexagonally packed *p6mm* space group. The scattering profile is consistent with a poorly ordered hexagonal symmetry. The in-plane cylinder-to-cylinder distance is approximately 23 nm, and the out-of-plane interlayer spacing is approximately 39.8 nm ($\sqrt{3}$ larger than in-plane distance). There is a strong halo from misoriented planes. However with the addition of 5 wt % DMSO/DOP (PR-5), there is a dramatic change in the scattering profiles as shown in Figure 2B with improvements in the definition of the diffraction peaks (in-plane *d*-spacing of 22 nm) and the appearance of higher order reflections in q_z. The disappearance of the halo in the scattering profile indicates the ordering has been significantly improved with preferred in plane alignment of the cylinders. The scattering pattern in Figure 2B is consistent with the *c2mm* space group (out-of-plane *d*-spacing is only 90% of that expected for *p6mm* due to contraction during thermopolymerization). There is further improvement in long-range order with increasing DMSO and DOP concentrations for PR-20 (Figure 2C) as evidenced by an increase in diffraction peaks visible in the GISAXS profiles, but these peaks include Debye−Scherrer rings;[45] these rings are typically associated with powder-like orientation, but this could also be associated with thickness variation of the films as the samples measured were small. Interestingly, PR-20 (Figure 2C) exhibits more higher order diffraction peaks than observed for the best analogous SVA film[33] after thermopolymerization. This highly selective solvent additives approach may not only be scalable for commercialization, but also provides advantages in sample ordering over SVA.

Despite the significant differences in the film thickness and scattering profiles, the in-plane *d*-spacing is quantitatively only slightly changed from 23 to 22 nm from PR-0 to PR-5 or PR-

dx.doi.org/10.1021/la401505h | Langmuir 2013, 29, 8703−8712

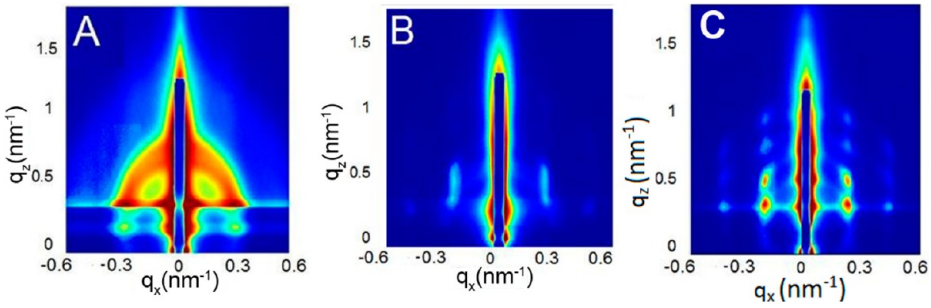

Figure 2. GISAXS patterns using 13.5 keV radiation after thermopolymerzation at 160 °C with different initial solvent additive content (A) 0 wt % at α_i = 0.11°, (B) 5 wt % at α_i = 0.1°, and (C) 20 wt % at α_i = 0.12°.

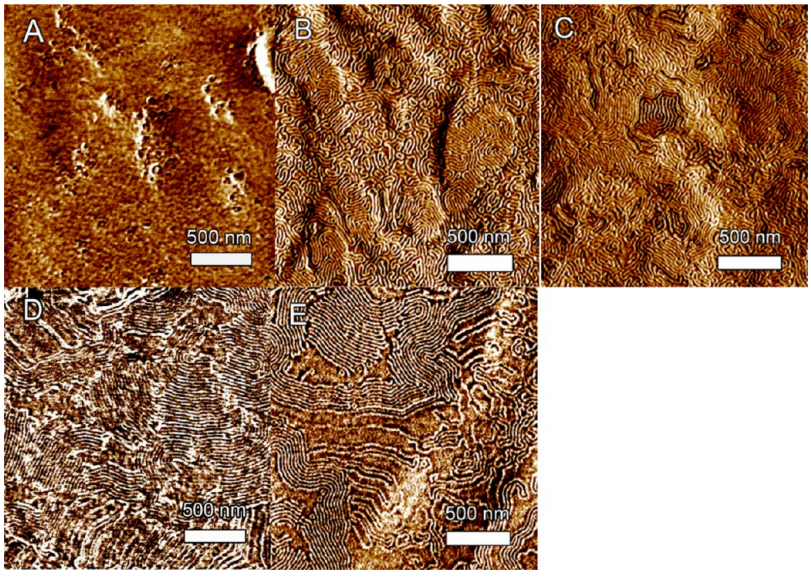

Figure 3. AFM phase images of the films with different initial concentrations of low volatility solvent additives (DMSO:DOP, 4:1) (A) 0 wt %, (B) 5 wt %, (C) 10 wt %, (D) 15 wt %, and (E) 20 wt % after template removal at 400 °C in a N_2 atmosphere.

20. This decrease in the *d*-spacing is counter to the 7% and 23% increase in thickness for PR-5 and PR-20, respectively, in comparison to PR-0. However, it is not unusual for a more disordered sample to have a larger *d*-spacing. Due to contraction during thermopolymerization and the preferred alignment of the cylindrical mesostructure with the addition of DMSO and DOP, the thickness of the unit cell in the out-of-plane direction also decreases from 39.8 to 34.3 to 33.5 nm for PR-0 to PR-5 to PR-20 (from geometry for perfect hexagonal packing, the out-of-plane *d*-spacing should be $\sqrt{3}$ larger than the in-plane *d*-spacing based on the orientation of the lattice from the interfaces, see the Supporting Information for additional details). However, there is a continual improvement in the long-range order and orientation of the films as the concentration of low volatility solvents increases; this change from a non-close-packed to close-packed structure may obfuscate the swelling of the *d*-spacing by the addition of solvent. Nonetheless, the *d*-spacing is not increased by the addition of the low volatility solvents, which is counter to typical observations for mesoporous carbon powders.[37] However, homopolymers can effectively swell the *d*-spacing and pore size for powders[38] but not thin films[32] due to segregation of the homopolymer to the film surface. Thus, it is not clear if this solvent additive methodology is able to modulate the pore size. As selective solvents for both the hydrophilic and hydrophobic domains are used, it is unusual that there would be no difference in the *d*-spacing.

To begin to understand the impact of the solvent additives on the pore structure, the surface morphology after calcination at 400 °C under N_2 is examined using AFM as shown in Figure 3. Under these conditions, the PS-*b*-PSS-DMODA block copolymer template[33] and residual solvents (DMSO and DOP) are completely removed. Without solvent additives (PR-0), very limited mesostructures can be observed (Figure 3A). There appears to be a common length scale for the light and dark domains in the micrograph, but no ordered structure is apparent, consistent with the diffraction profile for the thermopolymerized film (Figure 2A). In contrast, the addition of a small concentration of DMSO and DOP to the casting solution dramatically impacts the surface morphology. For PR-5 shown in Figure 3B, the surface morphology is almost a fingerprint pattern with very short correlations of the cylindrical mesopores on the surface. This improved clarity in the surface morphology is consistent with the GISAXS data for the precursor film (Figure 2B), where weak second order diffraction peak is present in q_x. As the solvent additive content increases to 10 wt %, the cylinders on the surface become longer on average, but long-range order of the mesostructure is still not very well-defined. With further increases in the solvent additive concentration, longer-range cylinder structures are visible in the surface morphology with continued coarsening of

dx.doi.org/10.1021/la401505h | *Langmuir* 2013, 29, 8703−8712

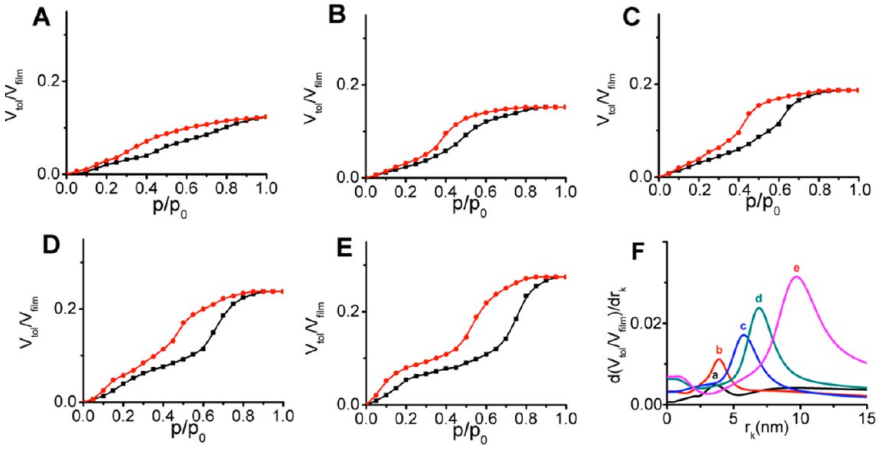

Figure 4. Absorption (■)−desorption (●) isotherms of mesoporous polymer thin films calcined at 400 °C as a function of initial content of mixed additive (A) 0, (B) 5, (C) 10, (D) 15, and (E) 20 wt %. There is a clear shift in the isotherms associated with changes in the pore size distribution (E), which is calculated from adsorption curve by application of the Kelvin equation. The lettering labeling the pore size distributions corresponds to the initial content of mixed additive as the isotherm panels.

the ordered grains. Interestingly, the progression in surface morphology as the additive concentration increases (Figure 3A to 3E) is reminiscent of the evolution in the surface morphology of neat block copolymers upon thermal annealing.[46] However, in this case, all the films have been exposed to the same thermal treatment (160 °C for 24 h). These AFM micrographs clearly illustrate the kinetic challenges with ordering this PS-*b*-PSS-DMODA/resol system. Addition of DOP at 20 wt % alone leads to no improvement in the ordering of the films, while 20 wt % DMSO provides some mobility for ordering (see the Supporting Information). However, the combination of the residual solvents (DMSO and DOP) during thermopolymerization at 160 °C provides significant mobility to the polymer segments to enable coarsening of the self-assembled structure prior to arrestment of structural reorganization from the cross-linking of the resol.

In addition to the changes in the mesostructure ordering, the micrographs in Figure 3 also allow differences in the pore size based upon the initial solvent additive concentration to be determined. The dark regions are the pores in the surface of the film, from which the pore diameter can be estimated. As the structure is poorly defined for PR-0, no pore diameter can be estimated. However for the other samples, there is a clear increase in the width of the pores as the solvent additive content is increased with the pore diameter growing from 4.8 ± 0.4, 6.6 ± 0.3, 7.7 ± 0.4, to 10.5 ± 0.3 nm for PR-5, PR-10, PR-15, and PR-20, respectively. These changes in the cylinder width suggest that the solvent acts to swell the hydrophobic PS domains through the cross-linking process.

To further investigate the differences in these mesoporous films and provide additional insight into any changes in pore size, adsorption and desorption isotherms of the films calcined at 400 °C are measured using ellipsometric porosimetry (EP). The refractive index of the film, *n*, is tracked as a function of the relative vapor pressure of toluene during EP from which the volume fraction of toluene absorbed is calculated using the Lorentz−Lorenz effective medium approximation (EMA) as[40]

$$\frac{V_{tol}}{V_{film}} = \frac{\left(\frac{n^2-1}{n^2+2}\right) - \left(\frac{{n_0}^2-1}{{n_0}^2+2}\right)}{\left(\frac{{n_{tol}}^2-1}{{n_{tol}}^2+2}\right)}$$

where n_0 and n_{tol} are the refractive indices (at 632 nm) of empty mesoporous films and condensed toluene, respectively. We assume the refractive index of toluene in the mesopores is the same as the bulk (1.496). Figure 4 illustrates the change in V_{tol}/V_{film} for both adsorption and desorption isotherms for the calcined films. For PR-0, V_{tol}/V_{film} increases continuously (Figure 4A) during adsorption with no apparent plateau in the isotherm. Thus, it is unclear if all of the pores in the film are filled during the EP measurement. Upon desorption, there is a large hysteresis loop, but the mesopores empty over a broad partial pressure range. This broad desorption (Figure 4A) correlates well with the poorly ordered morphology for PR-0 (Figures 2A and 3A) as the lack of order leads to a distribution of window sizes to enable desorption from the cylindrical mesopores (ink bottle effect).[47−49] By addition of DMSO and DOP to the casting solution, the adsorption and desorption isotherms are altered significantly. First, V_{tol}/V_{film} plateaus at high p/p_0, which suggests that all of the pores are filled. Second, a kink in the adsorption isotherm associated with the mesoporous ($0.45 < p/p_0 < 0.75$) becomes more pronounced and sharpens as the solvent additive concentration increases. Third during desorption, the mesopores empty in a relatively narrow relative partial pressure. With increasing the mass fraction of the solvent additives, the hysteresis loop in the desorption isotherms also becomes sharper. These characteristics of the sorption isotherms have been shown to be associated with an enhanced order structure in the mesoporous film,[42] which is consistent with the AFM micrographs for the surface topology (Figure 3).

In addition to this qualitative assessment of the sorption isotherms, quantitative values can be extracted relating to the film porosity, pore size distribution and surface area. If we assume that all of the pores in the film are filled during the adsorption isotherm, the maximum V_{tol}/V_{film} is equivalent to the film porosity as listed in Table 1. This increasing porosity is consistent with an increased pore volume due to swelling of the hydrophobic domains.

To further substantiate this increase in pore size, the Kelvin equation is applied to the adsorption isotherms to provide an estimate of the pore size distribution.

dx.doi.org/10.1021/la401505h | *Langmuir* 2013, 29, 8703−8712

Table 1. Characteristics of Mesoporous Films Calcined at 400 °C as Determined from Ellipsometric Porosimetry

sample	thickness (nm)	porosity (%)	$\langle r_k \rangle$ (nm)	surface area[a] (m^2/cm^3)
PR-0	440	12.2	3.1	42.3
PR-5	450	15.3	4.3	37.0
PR-10	465	19.9	5.8	44.5
PR-15	475	24.2	7.0	51.6
PR-20	485	28.1	9.9	68.9

[a]These surface areas may significantly underestimate the actual surface area for the mesoporous films due to uncertainties associated with parameters in this calculation. The relative differences in surface area should be representative of the added surface area from the addition of DMSO.

$$\frac{2}{r_k} = \frac{1}{r_1} + \frac{1}{r_2} = -\frac{RT}{\gamma V_L \cos\theta} \ln\left(\frac{P}{P_0}\right)$$

where r_k is the Kelvin radius, r_1 and r_2 are the radius of curvature of meniscus, R is the gas constant, T is the temperature, γ is the surface tension of toluene, V_L is the molar volume of the toluene, and θ is the contact angle of toluene. Assuming the physical properties of toluene are unchanged from the bulk, γ is 0.0284 N m^{-1}; V_L is 1.064×10^{-4} m^3 mol^{-1}; and contact angle is ~0°. The derivative of the volume fraction of absorbed toluene with respect to r_k provides an estimate of the pore size distribution as shown in Figure 4F. Without any additives, there is a broad pore size distribution with a small peak at approximately r_k = 3.1 nm. The pore size distribution is narrowed using additives with a relatively sharp Gaussian distribution in each case. The average r_k increases with increasing DMSO/DOP concentration (Table 1). One interesting result is that although the *d*-spacing of the in-plane structure decreases slightly from PR-0 to PR-20, the pore size increases by more than 300%. This large difference between the scattering spacing and pore size is quite unusual as the same fraction of solids (resol and PS-*b*-PSS-DMODA) is present in all the casting solutions. This is significantly different from two previous reports using trimethylbenzene[37] or polystyrene[38] as the swelling agent where both the *d*-spacing and pore size increased substantially with addition of the swelling agent. One explanation for this difference in behavior is the use of two selective solvents (DMSO and DOP) that maintain a constant hydrophilic − hydrophobic ratio in the films. Nonetheless, these larger pore sizes are consistent with the surface structure of these films as determined by AFM where the pore size from AFM of PR-20 (10.5 ± 0.3 nm) corresponds well to the average pore size from porosimetry (9.9 nm). Note that r_k is equivalent to the diameter for cylindrical mesopores. Moreover, the surface area of the mesoporous films can be estimated from *t* plots by application of the following equation:

$$S_{TOT} = \beta_{TOT} \frac{\rho_L}{\rho_G}$$

where ρ_L and ρ_G are densities of the adsorbate (toluene) in liquid and gas states. β_{tot} is the slope of *t* plot (see the Supporting Information) at low relative vapor pressures, which represents the change in volume of the absorbed toluene as a function of the thickness of absorbed toluene layer.

This methodology has been utilized previously to assess the surface area of silica with water as the adsorbate,[41] but the surface areas for the films are significantly underestimated due to uncertainties in ρ_L and ρ_G for water. For the mesoporous polymers examined here, the calcined resol can swell slightly with the exposure to toluene, so the adsorbed layer thickness is another source of uncertainty in addition to ρ_L and ρ_G. Table 1 provides the calculated surface areas from EP with the surface area varying from 37.0 to 68.9 m^2/cm^3. These calculated values are extremely low when compared to mesoporous powders with similar pore sizes. Even with 26 nm pore size, the surface area of mesoporous resol template by poly(ethylene oxide)-block-polystyrene is greater than 500 m^2/g.[18] This probable large underestimate of the surface area for the EP measurements is consistent with results for surfactant template (CTAB and F127) mesoporous silicate films where a surface area of approximately 200 m^2/cm^3 is reported,[41] but the analogous powders have surface areas exceeding 750 m^2/g.[50,51] Nonetheless, the relative differences in the surface areas can be qualitatively assessed by this analysis.

Examination of the surface areas carefully demonstrates a decrease with addition of DMSO/DOP for PR-5 in comparison to PR-0 with the surface area decreasing by 12.5%. However for larger concentrations of DMSO/DOP, we observe an increase in the surface area; for example, the surface area increases by 62.9% from PR-0 to PR-20. However, from examination of the t-plots for these films (see the Supporting Information), there is no apparent micropore volume in any of these films. This lack of micropore volume might be expected based upon the large size of the toluene probe molecule relative to N_2 that is typically used for bulk porous powders, but neutron scattering has illustrated micropores in mesoporous silicates can be filled by toluene.[52] However, this increase in surface area can be easily explained from simple geometry as the *d*-spacing remains constant, while the pore size increases. For perfect 2D hexagonal symmetry of infinite cylindrical mesopores, the specific surface area per unit volume, $A_{surface}$, can be calculated as

$$A_{surface} = \frac{2\pi R(1-P)}{([\sqrt{3}/2]a^2 - \pi R^2)}$$

where R is the pore radius, P is the film porosity, and a is the unit cell parameter for direct comparison to the EP measurements. Assuming that a is approximately 23 nm in all cases and that $\langle r_k \rangle$ = 2R, the surface areas can be predicted to increase as the pore size increases with surface areas of 25.8 m^2/cm^3 predicted for PR-5, 33.8 m^2/cm^3 for PR-10, and 58.6 m^2/cm^3 for PR-20. These geometric arguments provide the same trend for increased surface area of these ordered mesoporous carbon films as determined from the EP measurements; Sanchez and co-workers found similar agreement previously for mesoporous silica films with an *Im*3*m* morphology,[40] but the surface areas were much less than expected for analogous powders.[40,49] The decrease in surface area from PR-0 to PR-5 is attributed to the poor ordering and broad pore size distribution in PR-0 that increases the surface area due to defects in the cylindrical mesostructure from short cylinders and grain boundaries.

Mesoporous polymer can be converted to carbon by increasing the temperature to 800 °C in N_2. The corresponding loss of oxygen and hydrogen from the films during carbonization leads to significant contraction in the films. For example, the thickness of the PR-0 film decreases from 800 to 220 nm (73% contraction) from the as-spun stage to the carbonized state. Despite this substantial contraction in thickness, ordered

dx.doi.org/10.1021/la401505h | *Langmuir* 2013, 29, 8703−8712

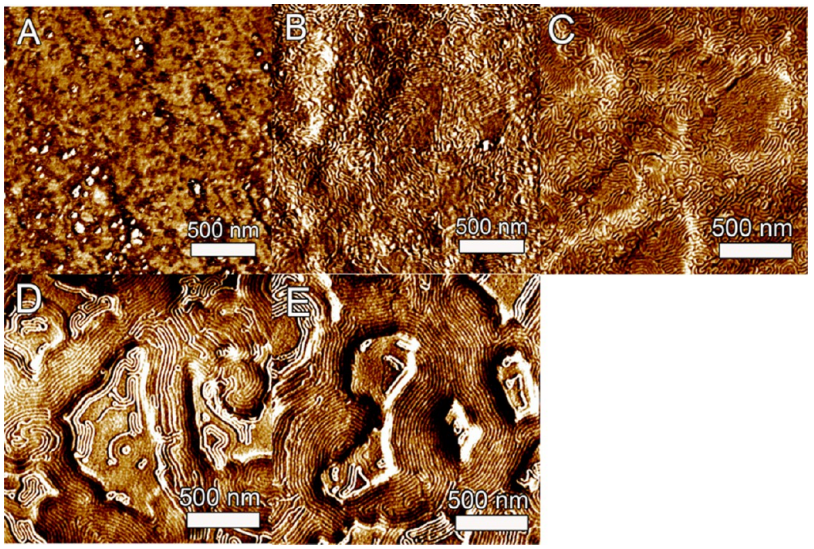

Figure 5. AFM phase images of the films with different initial solvent additive content (A) 0, (B) 5, (C) 10, (D) 15, and (E) 20 wt % after carbonization at 800 °C.

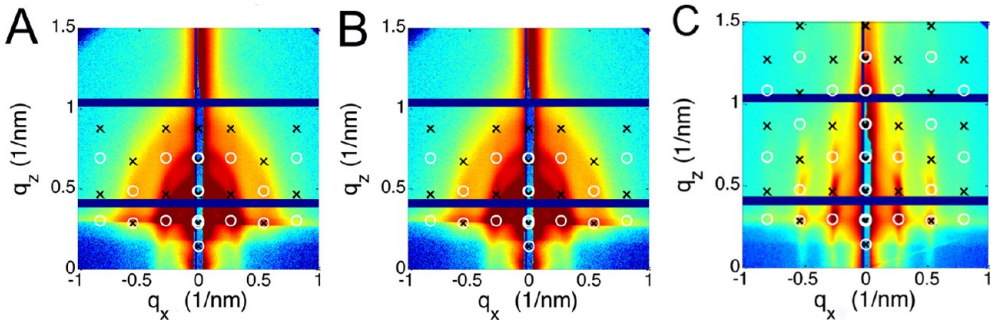

Figure 6. GISAXS pattern at $\alpha_i = 0.22°$ using 7.35 keV radiation for carbonized thin films with different initial content of solvent additives (DMSO and DOP). (A) 0, (B) 5, and (C) 20 wt %. X's and O's mark the predicted positions of Bragg peaks.

structures remain in the film. Figure 5 illustrates the surface morphology of the carbonized films. For the carbonized PR-0 film (Figure 5A), a very limited ordered structure is observed on the surface of the film. However, by increasing the content of the additives (DMSO and DOP), a well-defined cylindrical morphology develops with longer ranged ordering at high concentrations (Figure 5B–E). The contrast of the phase images also increases due to increased surface hydrophobicity of the carbon, which decreases the water meniscus at the tip–surface interface after carbonization. For the ordered films, the average pore diameter of carbonized films can be determined by measuring the width of darker surface regions from AFM phase images. As the concentration of DMSO and DOP increase (PR-5, PR-10, PR-15, to PR-20), there is a concurrent increase in the size of the surface pores from 3.9 ± 0.3, 5.4 ± 0.4, 6.8 ± 0.6, to 9.5 ± 0.5 nm, respectively. This trend is consistent with the pore sizes determined for the calcined films. However, there is a decrease in the size of these surface domains upon carbonization of approximately 1 nm. This decrease in lateral dimension is independent of the initial pore size, but does suggest that there is some mobility for rearrangement even after calcination. This slight shift in pore size is inconsistent with the traditionally held view of unidirectional contraction for mesoporous films,[53,54] but this block copolymer-resol system appears to disobey other commonly held conventions for mesoporous films such as EISA.[26]

To further quantify the ordered structure of the carbonized films, Figure 6 shows the GISAXS patterns for the PR-0, PR-5 and PR-20 films after carbonization. The diffraction peaks from the GISAXS patterns are fit as illustrated by the symbols following established methods for GISAXS analysis of nanostructured films.[55] For the PR-0 sample (Figure 6A), a strong ring is observed, indicating out-of-plane disorder, which is consistent with the films after thermopolymerization (Figure 2A). By adding 5% of the mixed additives, the GISAXS pattern is similar that the analogous film after thermal annealing, which shows the improvement in the order especially in the out-of-plane direction. For the PR-20 sample, there is a decrease in the number of higher order peaks compared to after thermal annealing. However, strong peaks are still observed in GISAXS pattern along the out-of-plane axis, demonstrating that 20% additive loading generates a layered structure. Also, the in-plane *d*-spacing of the PR-0 film (23.5 nm) and PR-20 (24 nm) after carbonization is nearly invariant, consistent with the scattering from films after thermopolymerization at 160 °C. Interestingly, the out-of-plane lattice parameter (d_z, thickness of unit cell) consistently scales with the in-plane *d*-spacing (d_x) irrespective of the solvent content; for a perfect *p6mm* (hexagonal) mesostructure, d_z should be a factor of $\sqrt{3}$ larger than d_x, but contraction of the lattice during carbonization leads to a 30%

dx.doi.org/10.1021/la401505h | *Langmuir* 2013, 29, 8703–8712

decrease in d_z. This distortion in the lattice is less than has been typically reported for soft template mesoporous carbons, where contraction of greater than 60% in d_z has been reported.[54] The significant expansion in the pore size without increasing the *d*-spacing as well as the decreased contraction in the film thickness in comparison to other methods could prove beneficial for membranes as the porosity can be enlarged to provide enhanced flux.

The use of two low volatility, selective solvents in the casting solution provides a novel route to tune the pore size and surface area, while also significantly improving the long-range ordering in these mesoporous carbon films. Unlike typical addition of a low volatility hydrophobic solvent to swell the pore size and the *d*-spacing, the pore size increases without a significant change in the *d*-spacing when using both hydrophobic and hydrophilic low volatility solvents. This method may be extendable to self-assembly of sol gel metal oxides with nonionic surfactants to increase both the pore size and surface areas of these films.

CONCLUSIONS

In conclusion, we have demonstrated that addition of two low volatility solvents that are selective for the hydrophobic and hydrophilic components of an amphiphilic block copolymer/phenolic resin composite can dramatically enhance the long-range order. Even after carbonization of the film, multiple orders of diffraction can be observed with GISAXS at high solvent concentrations. From examination of the GISAXS patterns, the mesostructures of these films are more ordered than typical mesoporous carbon films[24] templated with smaller surfactants that lack strong ionic interactions. In addition to enhancing the long-range order in these films, the addition of these low volatility solvents impact the physical characteristics of the film. The hydrophobic component of the block copolymer that templates the mesopores is swollen with addition of solvent with more than 300% increase in pore size observed, while there is no appreciable change in the *d*-spacing for the films. At the same time, the surface area of the mesoporous films is increased to due invariance in the *d*-spacing as the pores swell. This increase in surface area and pore size with addition of both DMSO and DOP without an increase in *d*-spacing is counter to the typical behavior with only addition of a low volatility hydrophobic solvent that tends to increase the pore size and *d*-spacing while decreasing the surface area.

ASSOCIATED CONTENT

Supporting Information

Dewetting of the films at large additive content is illustrated with optical micrographs. AFM images illustrate the surface morphology of control experiments using only DOP or DMSO. Adsorption isotherms with *t* plots are included to illustrate the calculations for determining surface area. This material is available free of charge via the Internet at http://pubs.acs.org.

AUTHOR INFORMATION

Corresponding Author

*E-mail: vogt@uakron.edu. Phone: (330) 972-8608.

Notes

The authors declare no competing financial interest.

ACKNOWLEDGMENTS

The authors acknowledge financial support by the National Science Foundation under Grant No. CBET-0746664. G.E.S. acknowledge support by the National Science Foundation under Grant No. DMR-1151468. Use of the APS was supported by the U.S. DOE, Office of Science, Office of Basic Energy Sciences, under Contract No. DE-AC02-06CH11357. We thank Joe Strzalka and Jin Wang for GISAXS support at APS. The authors thank Sarang Bhaway, Gurpreet Singh, and Kevin Yager for their assistance with the GISAXS measurements at NSLS. Research was carried out in part at the Center for Functional Nanomaterials, Brookhaven National Laboratory, which is supported by the U.S. Department of Energy, Office of Basic Energy Sciences, under Contract No. DE-AC02-98CH10886

REFERENCES

(1) Ismail, A. F.; David, L. I. B. A review on the latest development of carbon membranes for gas separation. *J. Membr. Sci.* **2001**, *193* (1), 1–18.

(2) Mahurin, S. M.; Lee, J. S.; Wang, X.; Dai, S. Ammonia-activated mesoporous carbon membranes for gas separations. *J. Membr. Sci.* **2011**, *368* (1–2), 41–47.

(3) Zhang, Y. X.; Xu, S. C.; Luo, Y. Y.; Pan, S. S.; Ding, H. L.; Li, G. H. Synthesis of mesoporous carbon capsules encapsulated with magnetite nanoparticles and their application in wastewater treatment. *J. Mater. Chem.* **2011**, *21* (11), 3664–3671.

(4) Corma, A. From microporous to mesoporous molecular sieve materials and their use in catalysis. *Chem. Rev.* **1997**, *97* (6), 2373–2419.

(5) Yu, J. S.; Kang, S.; Yoon, S. B.; Chai, G. Fabrication of ordered uniform porous carbon networks and their application to a catalyst supporter. *J. Am. Chem. Soc.* **2002**, *124* (32), 9382–9383.

(6) Kim, J.; Lee, J. E.; Lee, J.; Yu, J. H.; Kim, B. C.; An, K.; Hwang, Y.; Shin, C. H.; Park, J. G.; Hyeon, T. Magnetic fluorescent delivery vehicle using uniform mesoporous silica spheres embedded with monodisperse magnetic and semiconductor nanocrystals. *J. Am. Chem. Soc.* **2006**, *128* (3), 688–689.

(7) Kim, T. W.; Chung, P. W.; Slowing, I. I.; Tsunoda, M.; Yeung, E. S.; Lin, V. S. Y. Structurally Ordered Mesoporous Carbon Nanoparticles as Transmembrane Delivery Vehicle in Human Cancer Cells. *Nano Lett.* **2008**, *8* (11), 3724–3727.

(8) Kang, D.-Y.; Lee, Y.; Cho, C.-Y.; Moon, J. H. Inverse Opal Carbons for Counter Electrode of Dye-Sensitized Solar Cells. *Langmuir* **2012**, *28* (17), 7033–7038.

(9) Endo, M.; Kim, C.; Nishimura, K.; Fujino, T.; Miyashita, K. Recent development of carbon materials for Li ion batteries. *Carbon* **2000**, *38* (2), 183–197.

(10) Chang, H.; Joo, S. H.; Pak, C. Synthesis and characterization of mesoporous carbon for fuel cell applications. *J. Mater. Chem.* **2007**, *17* (30), 3078–3088.

(11) Lu, A. H.; Schuth, F. Nanocasting: A versatile strategy for creating nanostructured porous materials. *Adv. Mater.* **2006**, *18* (14), 1793–1805.

(12) Ryoo, R.; Joo, S. H.; Kruk, M.; Jaroniec, M. Ordered mesoporous carbons. *Adv. Mater.* **2001**, *13* (9), 677–681.

(13) Lu, A. H.; Li, W. C.; Schmidt, W.; Schuth, F. Template synthesis of large pore ordered mesoporous carbon. *Microporous Mesoporous Mater.* **2005**, *80* (1–3), 117–128.

(14) Liang, C. D.; Hong, K. L.; Guiochon, G. A.; Mays, J. W.; Dai, S. Synthesis of a large-scale highly ordered porous carbon film by self-assembly of block copolymers. *Angew. Chem., Int. Ed.* **2004**, *43* (43), 5785–5789.

(15) Meng, Y.; Gu, D.; Zhang, F. Q.; Shi, Y. F.; Yang, H. F.; Li, Z.; Yu, C. Z.; Tu, B.; Zhao, D. Y. Ordered mesoporous polymers and homologous carbon frameworks: Amphiphilic surfactant templating

and direct transformation. *Angew. Chem., Int. Ed.* **2005**, *44* (43), 7053−7059.
(16) Meng, Y.; Gu, D.; Zhang, F. Q.; Shi, Y. F.; Cheng, L.; Feng, D.; Wu, Z. X.; Chen, Z. X.; Wan, Y.; Stein, A.; Zhao, D. Y. A family of highly ordered mesoporous polymer resin and carbon structures from organic-organic self-assembly. *Chem. Mater.* **2006**, *18* (18), 4447−4464.
(17) Wan, Y.; Shi, Y.; Zhao, D. Y. Supramolecular aggregates as templates: Ordered mesoporous polymers and carbons. *Chem. Mater.* **2008**, *20* (3), 932−945.
(18) Deng, Y.; Yu, T.; Wan, Y.; Shi, Y.; Meng, Y.; Gu, D.; Zhang, L.; Huang, Y.; Liu, C.; Wu, X.; Zhao, D. Y. Ordered mesoporous silicas and carbons with large accessible pores templated from amphiphilic diblock copolymer poly(ethylene oxide)-b-polystyrene. *J. Am. Chem. Soc.* **2007**, *129* (6), 1690−1697.
(19) Zhang, J. Y.; Deng, Y. H.; Wei, J.; Sun, Z. K.; Gu, D.; Bongard, H.; Liu, C.; Wu, H. H.; Tu, B.; Schuth, F.; Zhao, D. Y. Design of Amphiphilic ABC Triblock Copolymer for Templating Synthesis of Large-Pore Ordered Mesoporous Carbons with Tunable Pore Wall Thickness. *Chem. Mater.* **2009**, *21* (17), 3996−4005.
(20) Schuth, F. Non-siliceous mesostructured and mesoporous materials. *Chem. Mater.* **2001**, *13* (10), 3184−3195.
(21) Sanchez, C.; Boissiere, C.; Grosso, D.; Laberty, C.; Nicole, L. Design, synthesis, and properties of inorganic and hybrid thin films having periodically organized nanoporosity. *Chem. Mater.* **2008**, *20* (3), 682−737.
(22) Feng, D.; Lv, Y.; Wu, Z.; Dou, Y.; Han, L.; Sun, Z.; Xia, Y.; Zheng, G.; Zhao, D. Free-Standing Mesoporous Carbon Thin Films with Highly Ordered Pore Architectures for Nanodevices. *J. Am. Chem. Soc.* **2011**, *133* (38), 15148−15156.
(23) Tanaka, S.; Nakatani, N.; Doi, A.; Miyake, Y. Preparation of ordered mesoporous carbon membranes by a soft-templating method. *Carbon* **2011**, *49* (10), 3184−3189.
(24) Schuster, J.; Koehn, R.; Keilbach, A.; Doeblinger, M.; Amenitsch, H.; Bein, T. Two-Dimensional-Hexagonal Periodic Mesoporous Polymer Resin Thin Films by Soft Templating. *Chem. Mater.* **2009**, *21* (24), 5754−5762.
(25) Tanaka, S.; Nishiyama, N.; Egashira, Y.; Ueyama, K. Synthesis of ordered mesoporous carbons with channel structure from an organic-organic nanocomposite. *Chem. Commun.* **2005**, *16*, 2125−2127.
(26) Schuster, J.; Koehn, R.; Doeblinger, M.; Keilbach, A.; Amenitsch, H.; Bein, T. In Situ SAXS Study on a New Mechanism for Mesostructure Formation of Ordered Mesoporous Carbons: Thermally Induced Self-Assembly. *J. Am. Chem. Soc.* **2012**, *134* (27), 11136−11145.
(27) Brinker, C. J.; Dunphy, D. R. Morphological control of surfactant-templated metal oxide films. *Curr. Opin. Colloid Interface Sci.* **2006**, *11* (2−3), 126−132.
(28) Brinker, C. J.; Lu, Y. F.; Sellinger, A.; Fan, H. Y. Evaporation-induced self-assembly: Nanostructures made easy. *Adv. Mater.* **1999**, *11* (7), 579−585.
(29) Segalman, R. A. Patterning with block copolymer thin films. *Mater. Sci. Eng. R* **2005**, *48* (6), 191−226.
(30) Song, L. Y.; Feng, D.; Fredin, N. J.; Yager, K. G.; Jones, R. L.; Wu, Q. Y.; Zhao, D. Y.; Vogt, B. D. Challenges in Fabrication of Mesoporous Carbon Films with Ordered Cylindrical Pores via Phenolic Oligomer Self-Assembly with Triblock Copolymers. *ACS Nano* **2010**, *4* (1), 189−198.
(31) Deng, Y. H.; Yu, T.; Wan, Y.; Shi, Y. F.; Meng, Y.; Gu, D.; Zhang, L. J.; Huang, Y.; Liu, C.; Wu, X. J.; Zhao, D. Y. Ordered Mesoporous Silicas and Carbons with Large Accessible Pores Templated from Amphiphilic Diblock Copolymer Poly(ethylene oxide)-*b*-polystyrene. *J. Am. Chem. Soc.* **2007**, *129* (6), 1690−1697.
(32) Labiano, A.; Dai, M.; Young, W.-S.; Stein, G. E.; Cavicchi, K. A.; Epps, T. H., III; Vogt, B. D. Impact of Homopolymer Pore Expander on the Morphology of Mesoporous Carbon Films Using Organic-Organic Self-Assembly. *J. Phys. Chem. C* **2012**, *116* (10), 6038−6046.
(33) Qiang, Z.; Xue, J.; Cavicchi, K. A.; Vogt, B. D. Morphology Control in Mesoporous Carbon Films Using Solvent Vapor Annealing. *Langmuir* **2013**, *29* (10), 3428−3438.
(34) Hahn, H.; Chakraborty, A. K.; Das, J.; Pople, J. A.; Balsara, N. P. Order-Disorder Transitions in Cross-Linked Block Copolymer Solids. *Macromolecules* **2005**, *38* (4), 1277−1285.
(35) Cao, L.; Man, T.; Kruk, M. Synthesis of Ultra-Large-Pore SBA-15 Silica with Two-Dimensional Hexagonal Structure Using Triisopropylbenzene As Micelle Expander. *Chem. Mater.* **2009**, *21* (6), 1144−1153.
(36) Soler-Illia, G.; Crepaldi, E. L.; Grosso, D.; Sanchez, C. Block copolymer-templated mesoporous oxides. *Curr. Opin. Colloid Interface Sci.* **2003**, *8* (1), 109−126.
(37) Wickramaratne, N. P.; Jaroniec, M. Phenolic resin-based carbons with ultra-large mesopores prepared in the presence of poly(ethylene oxide)-poly(butylene oxide)-poly(ethylene oxide) triblock copolymer and trimethyl benzene. *Carbon* **2013**, *51*, 45−51.
(38) Deng, Y.; Liu, J.; Liu, C.; Gu, D.; Sun, Z.; Wei, J.; Zhang, J.; Zhang, L.; Tu, B.; Zhao, D. Ultra-Large-Pore Mesoporous Carbons Templated from Poly(ethylene oxide)-*b*-Polystyrene Diblock Copolymer by Adding Polystyrene Homopolymer as a Pore Expander. *Chem. Mater.* **2008**, *20* (23), 7281−7286.
(39) Lodge, T. P.; Pudil, B.; Hanley, K. J. The Full Phase Behavior for Block Copolymers in Solvents of Varying Selectivity. *Macromolecules* **2002**, *35* (12), 4707−4717.
(40) Baklanov, M. R.; Mogilnikov, K. P.; Polovinkin, V. G.; Dultsev, F. N. Determination of pore size distribution in thin films by ellipsometric porosimetry. *J. Vac. Sci. Technol. B* **2000**, *18* (3), 1385−1391.
(41) Boissiere, C.; Grosso, D.; Lepoutre, S.; Nicole, L.; Bruneau, A. B.; Sanchez, C. Porosity and mechanical properties of mesoporous thin films assessed by environmental ellipsometric porosimetry. *Langmuir* **2005**, *21* (26), 12362−12371.
(42) Li, X.; Song, L. Y.; Vogt, B. D. Tuning mechanical properties of mesoporous silicas using associating homopolymers/block copolymer blends as templates. *J. Phys. Chem. C* **2008**, *112* (1), 53−60.
(43) Noro, A.; Matsushita, Y.; Lodge, T. P. Gelation Mechanism of Thermoreversible Supramacromolecular Ion Gels via Hydrogen Bonding. *Macromolecules* **2009**, *42* (15), 5802−5810.
(44) Vogt, B. D.; Watkins, J. J. Phase Behavior of Diblock Copolymers Dilated with Light Alkanes: Influence of Solvent Compressibility on Upper and Lower Ordering Transitions. *Macromolecules* **2002**, *35* (10), 4056−4063.
(45) Busch, P.; Rauscher, M.; Moulin, J.-F.; Mueller-Buschbaum, P. Debye-Scherrer rings from block copolymer films with powder-like order. *J. Appl. Crystallogr.* **2011**, *44*, 370−379.
(46) Harrison, C.; Adamson, D. H.; Cheng, Z. D.; Sebastian, J. M.; Sethuraman, S.; Huse, D. A.; Register, R. A.; Chaikin, P. M. Mechanisms of ordering in striped patterns. *Science* **2000**, *290* (5496), 1558−1560.
(47) Klingstedt, M.; Miyasaka, K.; Kimura, K.; Gu, D.; Wan, Y.; Zhao, D.; Terasaki, O. Advanced electron microscopy characterization for pore structure of mesoporous materials; a study of FDU-16 and FDU-18. *J. Mater. Chem.* **2011**, *21* (35), 13664−13671.
(48) Gorka, J.; Jaroniec, M. Hierarchically porous phenolic resin-based carbons obtained by block copolymer-colloidal silica templating and post-synthesis activation with carbon dioxide and water vapor. *Carbon* **2011**, *49* (1), 154−160.
(49) Gorka, J.; Fenning, C.; Jaroniec, M. Influence of temperature, carbon precursor/copolymer ratio and acid concentration on adsorption and structural properties of mesoporous carbons prepared by soft-templating. *Colloid Surf. A* **2009**, *352* (1−3), 113−117.
(50) Zhao, D. Y.; Huo, Q. S.; Feng, J. L.; Chmelka, B. F.; Stucky, G. D. Nonionic Triblock and Star Diblock Copolymer and Oligomeric Surfactant Syntheses of Highly Ordered, Hydrothermally Stable, Mesoporous Silica Structures. *J. Am. Chem. Soc.* **1998**, *120* (24), 6024−6036.
(51) Liu, R.; Shi, Y.; Wan, Y.; Meng, Y.; Zhang, F.; Gu, D.; Chen, Z.; Tu, B.; Zhao, D. Triconstituent Co-Assembly to Ordered Mesostruc-

tured Polymer-Silica and Carbon-Silica Nanocomposites and Large-Pore Mesoporous Carbons with High Surface Areas. *J. Am. Chem. Soc.* **2006**, *128* (35), 11652−11662.
(52) Vogt, B. D.; Pai, R. A.; Lee, H. J.; Hedden, R. C.; Soles, C. L.; Wu, W. L.; Lin, E. K.; Bauer, B. J.; Watkins, J. J. Characterization of Ordered Mesoporous Silica Films Using Small-Angle Neutron Scattering and X-ray Porosimetry. *Chem. Mater.* **2005**, *17* (6), 1398−1408.
(53) Ortel, E.; Reier, T.; Strasser, P.; Kraehnert, R. Mesoporous IrO_2 Films Templated by PEO-PB-PEO Block-Copolymers: Self-Assembly, Crystallization Behavior, and Electrocatalytic Performance. *Chem. Mater.* **2011**, *23* (13), 3201.
(54) Tanaka, S.; Katayama, Y.; Tate, M. P.; Hillhouse, H. W.; Miyake, Y. Fabrication of continuous mesoporous carbon films with face-centered orthorhombic symmetry through a soft templating pathway. *J. Mater. Chem.* **2007**, *17* (34), 3639−3645.
(55) Stein, G. E.; Kramer, E. J.; Li, X.; Wang, J. Layering Transitions in Thin Films of Spherical-Domain Block Copolymers. *Macromolecules* **2007**, *40* (7), 2453−2460.